PAPER

A low-cost integrated biosensing platform based on SiN nanophotonics for biomarker detection in urine

D. Martens,[ab] P. Ramirez-Priego,[c] M. S. Murib,[ab] A. A. Elamin,[d] A. B. Gonzalez-Guerrero,[c] M. Stehr,[d] F. Jonas,[d] B. Anton,[e] N. Hlawatsch,[e] P. Soetaert,[f] R. Vos,[g] A. Stassen,[g] S. Severi,[g] W. Van Roy,[g] R. Bockstaele,[f] H. Becker, [ID][e] M. Singh,[d] L. M. Lechuga[c] and P. Bienstman [ID] *[ab]

We present a low-cost integrated nanophotonic lab-on-a-chip platform suitable for point-of-care (POC) biomarker analysis. The sensor chip included in the platform contains multiplexed Mach–Zehnder interferometers with an on-chip optical spectral analyser consisting of an arrayed-waveguide grating. The sensor chip is fabricated in silicon nitride material, which makes it compatible with consumer-electronics-grade sources and detectors, leading to the possibility of low-cost instrumentation. The nanophotonic sensor chip exhibits a detection limit of 6×10^{-6} RIU (Refractive Index Units), which is in the same order of magnitude as the reported values for state-of-the-art evanescent wave sensors. The sensor chip is biofunctionalised with specific bioreceptors and integrated into a polymer microfluidic cartridge. The POC instrumentation platform contains optical excitation and read-out sub-systems and dedicated on-board software for real-time analysis of patient samples. To demonstrate the versatility of the platform, we present results both on the detection of an antigen related to tuberculosis directly in urine samples using a laboratory prototype and on the detection of a protein biomarker (CRP) related to inflammation using the integrated instrument.

Introduction

Integrated evanescent field photonic biosensors are promising candidates for real-time qualitative and quantitative evaluation of biomolecular interactions. In these sensors, a change in the effective refractive index caused by the binding of an analyte to its specific bioreceptor is converted into a measurable quantity, most commonly a resonant wavelength shift, through an integrated photonic transducer. Various types of sensors have been developed: Young and Mach–Zehnder (MZI) interferometers, bimodal sensors, ring resonators, photonic crystal based sensors and various others.[1–5] In general, evanescent wave sensors provide sensitivity, selectivity and versatility, which makes them applicable in a broad range of disciplines, ranging from medicine and food quality control to environmental management. Furthermore, they offer great potential as lab-on-a-chip devices, performing point-of-care measurements at an affordable cost.

While practical applications have emerged, in many cases the readout of these sensors requires either an expensive tuneable laser or an off-chip spectrometer, making them expensive and/or slow. Therefore, the instrumentation cost is typically high, rendering the system unfit for true point-of-care applications. We aim to overcome this important barrier by using a broadband light source in combination with an on-chip spectral filter as the interrogation mechanism.[6–8] The filter divides the transducer spectrum into different wavelength channels with spatially separated output ports. By fitting a curve to this dataset, the central wavelength of the original sensor spectrum is determined with an accuracy that surpasses the resolution of the spectral filter itself by multiple orders of magnitude.

The manuscript is structured as follows. First, we present how such sensor chips can be designed and fabricated using mass-fabrication-compatible technology. Before moving on to a fully integrated platform with dedicated microfluidics and readout components, we first characterised the performance of the sensor chip in a lab-based prototype with in-house microfluidics. We determine the bulk limit-of-detection and then

[a]Photonics Research Group, Ghent University, Imec, Technologiepark-Zwijnaarde 15, B-9052 Ghent, Belgium

[b]Center for Nano- and Biophotonics (NB-Photonics), Ghent University, Ghent, Belgium

[c]Nanobiosensors and Bioanalytical Applications Group, Catalan Institute of Nanoscience and Nanotechnology (ICN2), CSIC, BIST, CIBER-BBN, Campus UAB, Bellaterra, 08193 Barcelona, Spain

[d]LIONEX Diagnostics and Therapeutics GmbH, Braunschweig, Germany

[e]Microfluidic ChipShop GmbH, Stockholmer Str. 20, D-07747 Jena, Germany

[f]Trinean NV, Dulle-Grietlaan 17/3, 9050 Gent, Belgium

[g]7 Imec, Kapeldreef 75, 3001 Leuven, Belgium

move further to perform biosensing experiments to detect *Mycobacterium tuberculosis* lipoarabinomannan (LAM) in clinical samples. After that, we move from a lab-based prototype to a fully integrated platform that is closer to commercialisation. We discuss how these silicon nitride based sensor chips can be integrated into a standard polymer fluidics cartridge, and describe in more detail the custom readout instrument and the associated software. Finally, this integrated platform is used to detect the C-reactive protein biomarker, related to inflammatory processes.

Photonic sensor design

The most important property for an integrated photonic sensor to enable use as a point-of-care diagnostic device is compatibility with a cheap read-out system, requiring no expensive components such as tuneable lasers or off-chip spectrometers. In our design, the approach is to interrogate the sensor through an off-chip broadband light source, an on-chip spectral filter and an off-chip camera, all of which are affordable in a point-of-care context. This is especially true for the very near-infrared wavelength range, which can be used due to the choice of sensor material. The spectral filter employed is an Arrayed Waveguide Grating (AWG), which is a state-of-the-art design in the given wavelength range (850 nm) in terms of footprint as well as performance.[9]

As a sensor for this interrogation scheme, a Mach–Zehnder Interferometer (MZI) was selected, with one of the arms isolated from and the other exposed to the analyte. The main merit of this MZI configuration is its large design freedom, which enables tuning the sensitivity and spectral period independently. The latter is relevant, as the characteristics of integrated spectral filters are typically restricted by fabrication limitations,[10] and their ratio has a large influence on the final performance of the sensor.[6] The light interfacing with the chip occurs through grating couplers. At the input side, the grating couplers are flood-illuminated by a broadband light source.[11] This method allows interrogating multiple sensors at the same time, and as such opens the door to multiplexing. At the output side, the transmitted power of a large number of grating couplers is measured in parallel with a camera. A picture of the complete design of the photonic sensing circuit is shown in Fig. 1.
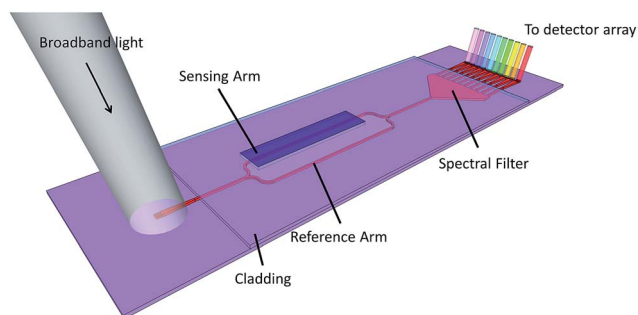

Fig. 1   Integrated photonic sensor circuit consisting of a MZI sensor read-out by an on-chip AWG spectral filter.

(a) Sensor spectrum   *(b) Sensor and filter channels*

(c) Discretized sensor data   *(d) Discretized sensor data, reconstructed spectrum and fitted spectral peak*
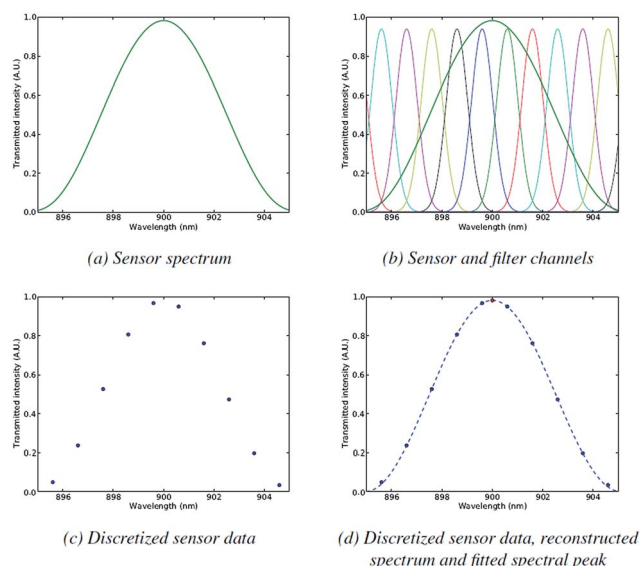
Fig. 2   Interrogation principle based on a broadband source and an on-chip spectral filter.

The transduction mechanism is based on the evanescent field: a change in the environment of the exposed MZI arm, such as a binding event or a bulk refractive index shift, will result in a change in the effective refractive index of the exposed MZI arm. This, in turn, results in a phase shift in this arm, which causes a spectral shift in the whole spectrum of the MZI. This shift is tracked through continuous monitoring of the locations of the spectral peaks of the MZI. To determine the peaks of this spectrum, we illuminate the chip using a broadband light source. The spectrum of the MZI sensor (Fig. 2a) is sent through the different channels of the spectral filter (Fig. 2b), yielding a discretised version of the sensor spectrum (Fig. 2c). The resolution of this spectrum is typically low, as it is limited by the number of available data points per spectral period, determined by the channel spacing of the on-chip spectral filter. To compensate for this drawback, the original spectrum is reconstructed from the discretised data through fitting (Fig. 2d), and the peak of this reconstructed spectrum is tracked. This greatly increases the accuracy of the obtained peak wavelength values. This procedure is more elaborately described in ref. 6. Compared to other interrogation mechanisms based on tuneable lasers, our approach with an integrated spectral filter allows the use of cheap LEDs, bringing the cost of the source from thousands of dollars to a few dollars or less.

The whole sensing chip contains 6 sensors, each of them with their MZI and AWG, as well as 30 output grating couplers per sensor, one for each of the AWG channels. The entire design fits in a chip area of less than 6 mm × 6 mm (Fig. 3).

Sensor fabrication

Photonic integrated circuit (PIC) sensors were fabricated based on the CMOS compatible SiN photonics developed at imec,
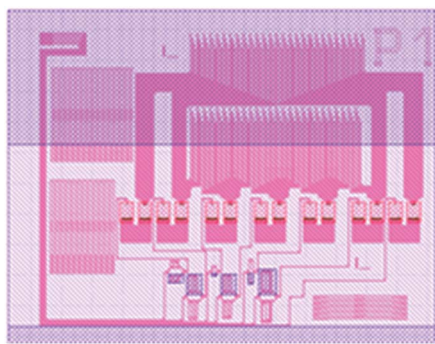
Fig. 3 Layout of a sensing circuit consisting of 6 sensors, each of them with their own MZI and AWG.

using wafer-level processing on standard 725 μm thick 200 mm Si wafers.[10] First a 70 nm thick SiN anti-reflective coating was deposited using plasma-enhanced chemical vapour deposition (PECVD) using SiH_4, N_2 and NH_3 at 400 °C (Fig. 4). The purpose of this layer is to decrease the back-reflections coming from the oxide–Si interface, which would reduce the light incoupling efficiency of the grating couplers. Subsequently, a 2.3 μm thick PECVD SiO_2 layer, which had been specifically engineered to compensate for the stress level of the wafers, was deposited using SiH_4 and N_2O. The roughness of the layer was reduced by applying a short chemical–mechanical polishing (CMP) step. On top of this oxide layer, a 220 nm thick PECVD SiN layer was deposited using SiH_4, N_2 and NH_3 at 400 °C. This waveguide material has been optimised to minimise the light propagation loss in the visible wavelength range.[10] Refractive indices at $\lambda = $ 850 nm were $n_{SiO_2} = 1.48$ and $n_{SiN} = 1.88$ as measured by ellipsometry.

Grating couplers were defined using 193 nm deep ultraviolet (DUV) lithography followed by a shallow etch of 110 nm depth

into the SiN to maximise light coupling into the waveguide. A fluorine-based inductively coupled plasma reactive ion etching process was used to minimise the sidewall roughness and achieve the required sidewall slope. Next, waveguides were defined by a separate 193 nm DUV lithography step and a similar etch, but now the full thickness of the SiN layer was etched. Following this process, a 2 μm layer of PECVD SiO_2 was deposited and planarised by CMP. Finally sensing regions were defined by lithography using the i-line of Hg at 365 nm followed by a selective removal of the top oxide cladding using a dry etching process followed by a wet etching step.

Evaluation of the bulk sensitivity

Sensors were initially characterised through bulk sensing in a lab-based setup, with equipment compatible with point-of-care sensing. The bulk sensing limit-of-detection (LOD) provides an excellent figure-of-merit as it can be compared between various sensor types regardless of surface bio-functionalisation. To evaluate this value, the sensor is exposed to different concentrations of a solution (*i.e.*: HCl) in alternation with water. An example of a resulting sensorgram, where 5 sensors are measured in parallel, is shown in Fig. 5.

To determine the LOD, the following procedure was used. The shifts of the spectra are tracked, and the sensitivity of each sensor is calculated as the slope of the obtained spectral shifts as a function of the corresponding changes in the bulk refractive index. The minimum detectable wavelength shift is calculated as 3 times the standard deviation on the signal after transients have passed. The ratio of minimum detectable wavelength shift to sensitivity yields the LOD. This experiment was done multiple times, with different chips from different wafers. The set of experiments yielded an average LOD of 6×10^{-6} RIU, with a standard deviation of 2×10^{-6} RIU. This indicates a high reproducibility (given that we used different chips) as well as results competitive with most integrated photonic sensors, despite the low-cost read-out.[6]
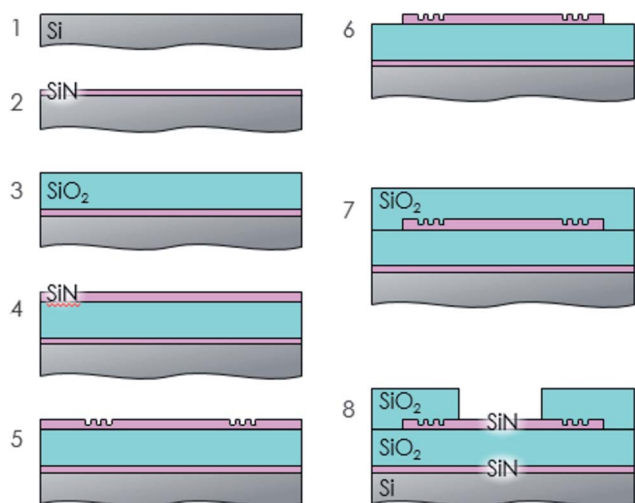

Fig. 4 Process flow for the SiN photonic chip fabrication. (1) Si substrate, (2) deposition of the anti-reflective coating, (3) deposition and chemical–mechanical polishing (CMP) of the bottom clad, (4) deposition of the SiN waveguide layer, (5) shallow etch of the grating couplers, (6) deep etch of the waveguides, (7) deposition and CMP of the top clad, and (8) clad-open etch.
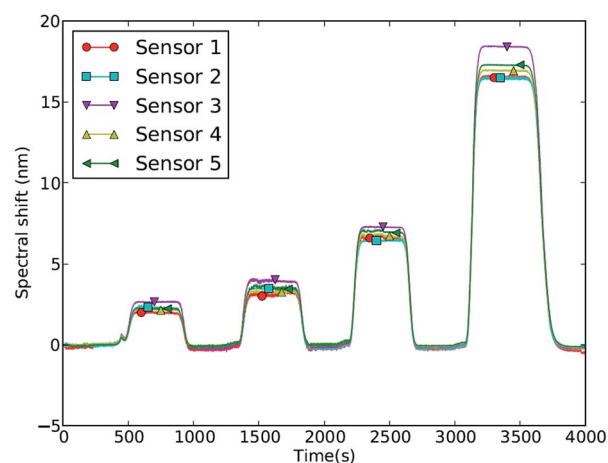

Fig. 5 Sensorgram of parallel measurement of five MZI sensors, where the sensors are exposed to different concentrations of HCl in alternation with water.

LAM detection in urine (lab setup)

Before building an integrated readout system with a dedicated microfluidic cartridge, we first tested the functionality of the sensor chip by performing LAM measurements in clinical urine samples. LAM is a biomarker indicative of tuberculosis (TB) infection,[12] and we correlated the measurements with the disease status of the participants. All experiments were performed in compliance with the relevant German and Spanish laws and institutional guidelines, and were approved by the Aerztekammer Niedersachen and the National Institute of Medical Research Tanzania. Informed consent was obtained.

To prepare the chips, anti-LAM IgM mAb molecules were covalently immobilised on the SiN chips using a silane route.[13,14] Prior to any functionalisation, the SiN chips were cleaned in acetone, isopropanol, and ultrapure water. Next, the chips were exposed to oxygen plasma for one minute using a reactive-ion etching (RIE) system to terminate the surface with hydroxyl groups. Afterwards, the silanisation of the chips was carried out by liquid-phase deposition of silanes in an organic solvent.[14] The chips were placed in a 600 mM solution of (3-amino-propyl)tri-ethoxysilane (APTES, 99%; Sigma-Aldrich, Steinheim, Germany) in toluene ($\geq$99.9%, Sigma-Aldrich) for 15 hours in a nitrogen-filled glove-box. To wash off unbound APTES molecules, the chips were rinsed with toluene, followed by tetrahydrofuran (THF, $\geq$99.9%, Sigma-Aldrich). After drying the chips under a nitrogen flow, they were cured for 30 minutes at 120 °C, resulting in an especially strong adhesion of the APTES layer to the surface.[14] This way, the surface becomes modified with amines, allowing for the subsequent reaction with succinic anhydride (SA) in order to yield a carboxyl-terminated surface.[13,15] Succinic anhydride (SA, $\geq$99.9%, Sigma-Aldrich) was used as a cross-linker molecule to ensure the binding of the amino group of APTES to the NH_2 groups of the anti-LAM by providing carboxylic groups at the surface. For this purpose, the chips were placed overnight in a solution of 800 mM SA in acetonitrile (ACN) (anhydrous, 99.8%, Sigma-Aldrich), after which they were rinsed with pure acetonitrile and dried under nitrogen gas. The amine-terminated surface reacts with one of the two carbonyl groups of the SA molecules, causing the anhydride ring to open and to form a covalent bond with this carbonyl group. The other carbonyl group is released to form a free carboxylic acid-terminated surface.[16] The anti-LAM molecules were randomly oriented and covalently coupled to the carboxyl-terminated SiN chips using the zero-length cross-linker 1-ethyl-3-3-dimethylaminopropyl-carbodiimide (EDC) in 2-[N-morpholino]-ethanesulphonic acid (MES) buffer at room temperature. We found experimentally that a twofold blocking layer with 0.5 mg mL^{-1} PLL(20)-g[3.5]-PEG(5) (SuSoS) and 10 mg mL^{-1} BSA-A7906 (Sigma-Aldrich) was required to avoid non-specific adsorptions when evaluating urine.

Fig. 6 shows the experimental setup used to perform the evaluations of urine samples. In this set-up, an external syringe pump is employed to pump fluids. A dual mode injector valve is used to load the samples to be tested in line with the neutral PBS buffer. During the experiment, first the buffer is flowed to
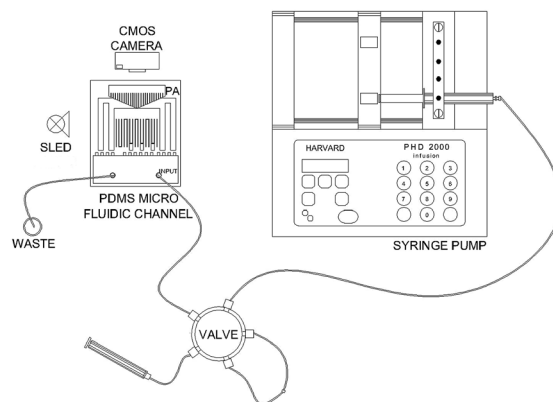

Fig. 6 Experimental setup of the lab-based prototype.

establish the baseline, then the clinical sample, followed by the buffer again to wash away any nonspecific binding. The sensor chip is squeezed under a home-made PDMS microfluidic channel. The light source is an 850 nm SLED. The signal is collected using a CMOS camera, which is connected to the computer to analyse the detected signal.

A series of urine samples of healthy and non-healthy persons were selected for experimental tests. Apart from testing the lab prototype, the use of actual urine samples also allows us to evaluate the effect of nonspecific binding. The samples were pumped into the microflow cell at a rate of 10 μL min^{-1} for 20 minutes. Results from four sensors on the chip were analysed.

Fig. 7a and b show the real-time interaction of urine of healthy and non-healthy persons with the anti-LAM molecules immobilised on the SiN sensors. First, 1× PBS (pH = 7) was administered to the sensors. After stabilisation of the signal, 200 μL of a urine sample was injected onto the sensors.

In the case of samples from healthy persons, initially a high spectral shift was encountered due to buffer exchange. This high spectral shift was only temporary and started to return to its starting value after a while since no LAM/anti-LAM binding was occurring. When 1× PBS was injected afterwards, the spectral shift moved back to a very low value (220 pm) as compared to the initial shifted value. The spectral shift did not completely return to its starting value and this can be attributed to nonspecific binding of residuals present in the urine samples to the sensor surface.

In the case of samples from non-healthy persons, a high increase in the spectral shift was encountered due to the buffer effect. However, afterwards, when the 1× PBS was injected, a high permanent spectral shift compared to its initial value was encountered. This is due to the fact that LAM was present in the urine and it efficiently bound to the anti-LAM immobilised on the sensor surface. In Fig. 7b, the non-healthy sample caused a permanent spectral shift of about 6 nm.

A series of urine samples from four healthy persons and four non-healthy persons was measured. The results are summarised in Table 1. A maximum permanent spectral shift of 0.85 nm was obtained for healthy persons. The samples from non-healthy persons caused a minimum permanent spectral shift
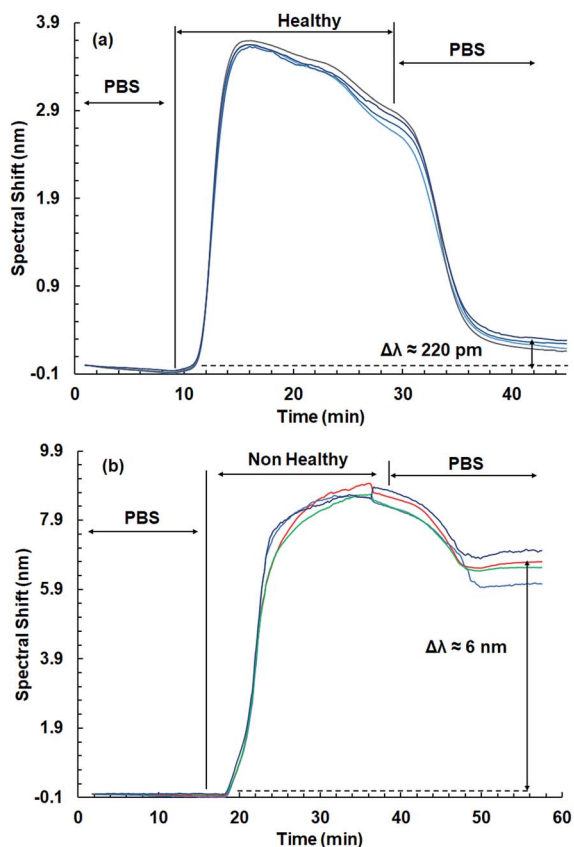
Fig. 7   Spectral shift for healthy (a) and non-healthy (b) persons.

Table 1   List of the spectral shift due to a series of samples from healthy and non-healthy persons

Sample type	Spectral shift
Healthy # 1	0.75 nm
Healthy # 2	0.85 nm
Healthy # 3	0.22 nm
Healthy # 4	0.50 nm
Non-healthy # 1	6.00 nm
Non-healthy # 2	5.50 nm
Non-healthy # 3	7.00 nm
Non-healthy # 4	4.00 nm

of 4 nm and a maximum permanent spectral shift of 7 nm, depending on the concentration of the LAM present in the urine samples. The permanent spectral shift obtained for samples of non-healthy persons is very high compared to the permanent spectral shift obtained due to the healthy samples. Moreover, as can be noticed from Fig. 7a and b, the shape of the sensorgrams in both cases is also very different: while the sample is still being injected, the spectral shift already starts to decrease for the healthy person sample, which is not the case for the non-healthy person sample.

Finally, the sensorgrams also show that an assay time of 10 to 15 minutes is feasible. Also worth noting is that the experiments were done at room temperature and that no sample preparation was performed.

Microfluidic cartridge

Microfluidic cartridge bodies were injection-moulded in COC (cyclo-olefin-polymer, trade name Topas). This allows for a cost-effective large-scale production, so that the cartridges can be made cheap enough to be disposable.

For the integrated cartridge design, an injection moulding platform of a microscopy slide format with a footprint of 75.5 mm × 25.5 mm was chosen. This format provides an easy-to-handle size on which all relevant fluidic and detection functionalities were accommodated, allowing for a high integration density with various functional elements for such a disposable cartridge.

A photograph of a microfluidic cartridge with the integrated photonic chip is depicted in Fig. 8.

For the inlet of the urine sample and required reagents, the integrated cartridge includes female Luer interfaces being compatible with standard syringes, as commonly used.

An integrated filter ensures the retention of coarse components from the urine sample and an integrated air bubble trap retains undesirable air bubbles. At the end of the fluidic path, a reservoir for easy liquid waste handling is placed, followed by an air vent to allow air to escape from the cartridge when the waste reservoir fills up.

With respect to the integration of the sensor chip, there is an appropriately designed recess on the top, while the rest of the cartridge is designed to leave parts of the chip exposed for easy optical access. Indeed, light is coupled into and out of the chip through grating couplers, and these need to stay exposed.

Fig. 9 shows an intersection through the sensor area of the microfluidic cartridge. Note that the photonic chip is positioned upside down and that the optical detection is performed from the bottom side.

Integrated readout instrument

The fabricated readout instrument is shown in Fig. 10. The POC platform includes the optical readout, the pumping unit interfacing with the cartridge, and a touch screen with the user interface. The size of the instrument is determined by the choice of using vertically oriented syringes to load the samples and the buffers.
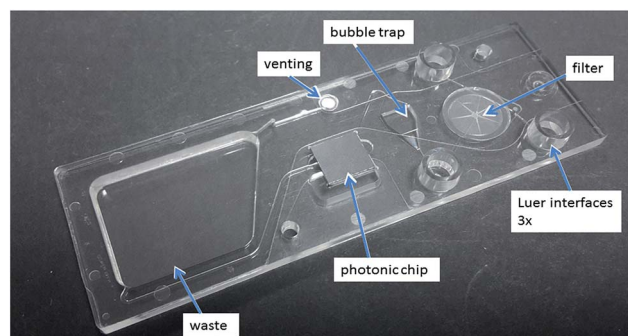

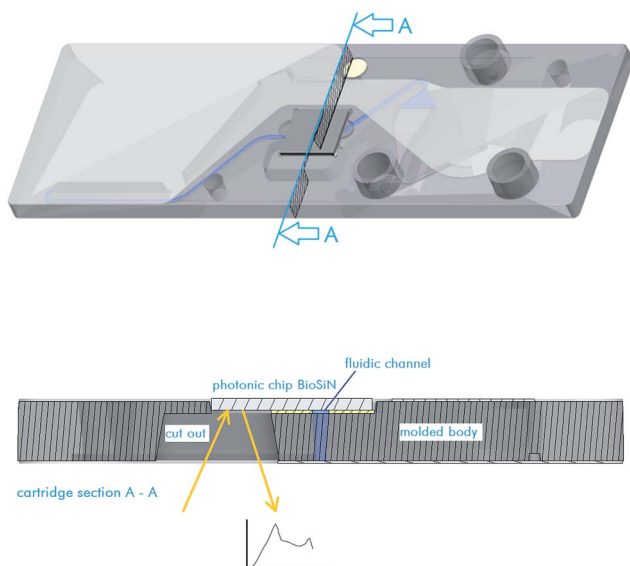Fig. 8   Assembled microfluidic cartridge.

Fig. 9 Cross section (bottom) through the microfluidic cartridge along section A–A (indicated in the top figure).
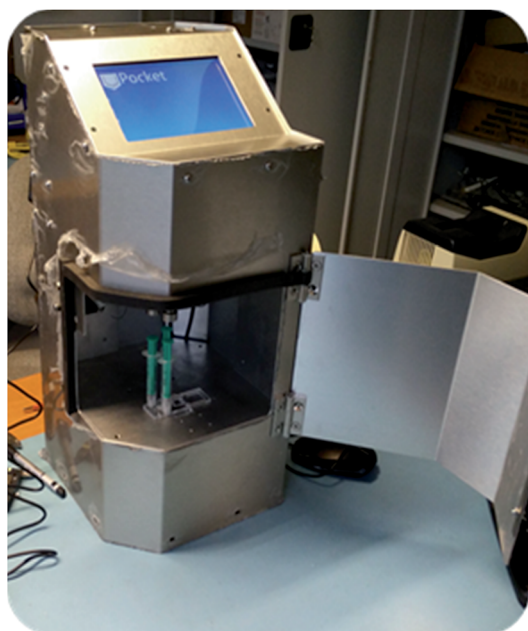

Fig. 10 Integrated readout instrument.

When designing the concept of this instrument, importance was given to flexibility, the possibility to test alternatives to specific parts, ease of assembly, ease of shipment and system installation at test sites. Likewise it should be noted that – although the readout architecture is selected to be low-cost – the prototype instrument design is also not yet optimised for cost. For example, the integration of the full Windows-PC including a high-resolution touch screen certainly adds to the cost of the system, but also offers flexibility to update software in a late stage of the development (testing) cycle.

The optical readout unit (Fig. 11) contains the light source as well as the light sensor to interrogate the optical biosensor chip.
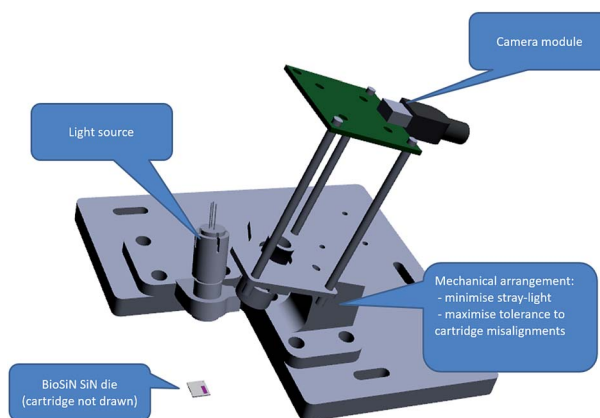

Fig. 11 Optical readout module (upside down).

The unit is mounted upside down in the bottom part of the instrument. The light source (SLED) and the detector (CMOS sensor) are both commercial off-the-shelf components, coupled to a custom lens system.

Three syringe pumps are integrated into the readout instrument (Fig. 12). Each pump has a stepper motor directly driving a piston up and down. The piston pushes the plunger of the syringe downwards, transferring the contents of the syringe (buffer, sample, …) to the cartridge. As the distance between the syringes is small, the piston axis is not in line with the stepper motor axis, but parallel. A dry bearing system is used to guide the piston up and down. The piston also includes a pressure sensor, to detect mechanical contact between the piston head and the syringe plunger. To increase confidence in the measurements, an extra flow monitoring system was also installed, consisting of a separate camera system to image the fluidic channel to perform bubble detection.

Custom software was written to reliably identify the position of the output grating couplers in the images captured by the CMOS sensor. The intensities of these spots are then used in a fitting procedure, which allows us to track the position of the peak wavelength as a function of time.

Fig. 13 shows a simple proof-of-concept sensing experiment on the instrument using the actual microfluidic cartridge, which measures the physical adsorption of BSA on an unfunctionalised sensor chip.
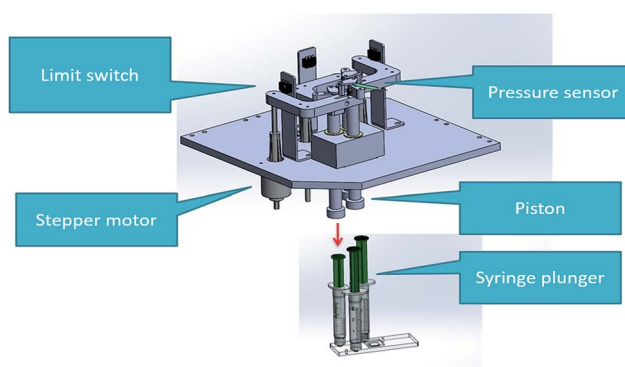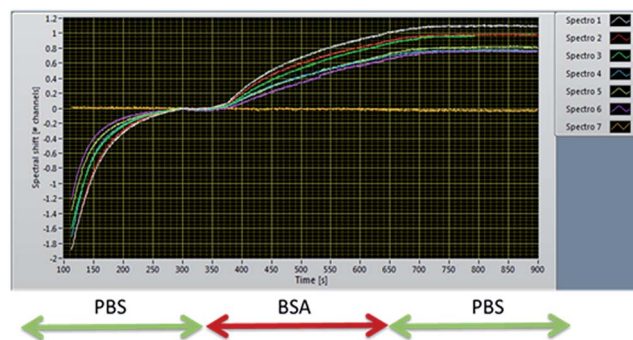

Fig. 12 Pump unit.

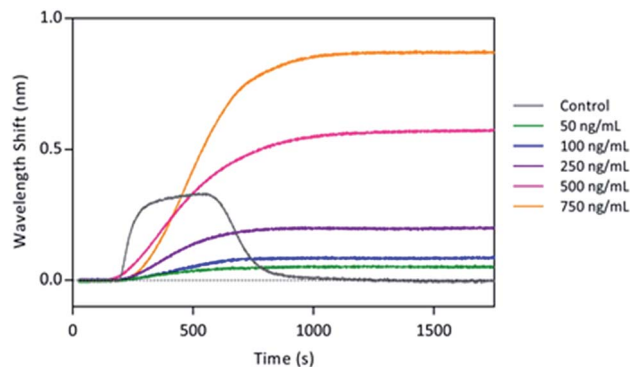Fig. 13 Physical adsorption of BSA using an unfunctionalised cartridge.

Fig. 14 Real-time monitoring of different CRP concentrations and BSA as a control with the biosensor instrument.

Biosensing with the integrated readout instrument

Finally, this setup was used to perform biosensor experiments using functionalised chips. As a model system to test the prototype, the immunosensing of the C-reactive protein (CRP) biomarker was chosen. CRP is a widely used biomarker in patients that plays an essential role as an early indicator of inflammation and infection, and is also used as an indicator of prognosis for cardiovascular disease.[17,18] CRP concentration in serum under healthy conditions is lower than 10 μg mL^{-1} and it can increase up to 200 μg mL^{-1} in the case of inflammation or infection. CRP can be detected through interaction with its specific antibody. As a proof-of-concept, here we focus on the easier case of CRP detection in buffer.

Monoclonal antibody anti-human C-reactive protein C7 produced in mouse and human CRP was purchased from HyTest (Finland) and BBI Solutions (UK), respectively. All chemical reagents were purchased from Sigma-Aldrich (Germany).

50 μg mL^{-1} anti-CRP in phosphate buffered saline (PBS; 10 mM phosphate, 137 mM NaCl, 2.7 mM KCl, pH 7.4) was immobilised onto the surface of the chip through physical adsorption, followed by a 10 mg mL^{-1} bovine serum albumin (BSA) solution to block the free sensor surface. Milli-Q water (Millipore, US) was used as a running buffer for the immobilisation and blocking steps. For the CRP protein detection, the running buffer was changed to PBS to ensure optimal conditions for the immunosensing interaction, as well as to maximise the stability of the bioreceptor layer.

In an immobilisation strategy based on electrostatic interactions, it is not possible to remove the CRP protein bound to the antibody due to its weak attachment to the sensor surface and thus an additive immunosensing assay was employed to establish the analytical calibration curve for the CRP detection. To study the biointeraction between CRP and its specific antibody, successive dilutions of increasing CRP concentrations (50, 100, 250, 500 and 750 ng mL^{-1}) were flowed over the sensor area. A direct relationship between the concentration and the sensor response can be observed (Fig. 14). Furthermore, the specificity of the immunoassay was analysed by injecting
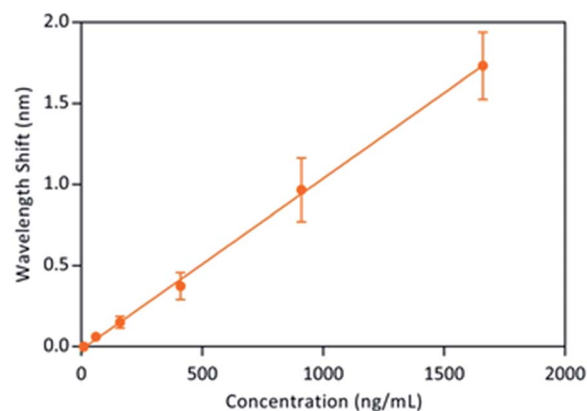

Fig. 15 Calibration curve for the detection of CRP in PBS.

a control of 1000 ng mL^{-1} BSA instead of CRP, resulting in a negligible response of the sensor, as shown also in Fig. 10.

As shown in Fig. 15, a detection curve was obtained by plotting the accumulated response signal as a function of the accumulated CRP concentration. The limit of detection (LOD) was determined from the calibration curve as three times the standard deviation of the signal. The resulting LOD was 19.478 ng mL^{-1} ($R^2 = 0.9701$) which theoretically corresponds to the lowest detectable CRP concentration. These results indicate that the integrated instrument and the designed photonic sensor could be used as an effective biosensor for CRP detection as the concentration of this biomarker when related to infection or disease is much higher than the one obtained.

Conclusions

We presented an integrated sensor platform that allows low-cost detection of various biomarkers. The sensor chip with an integrated spectral filter eliminates the need for an expensive tuneable laser so that a cheaper broad-band light source can be used. A technology to integrate this chip into a microfluidic cartridge was presented, together with the development of a dedicated readout instrument. We presented proof-of-concept results for the detection of LAM in actual clinical urine samples

as well as for the detection of CRP. These results show the feasibility of using this system as a promising platform technology to detect different kinds of biomarkers using a cheap readout instrument.

Conflicts of interest

There are no conflicts to declare.

Acknowledgements

References

1 A. F. Gavela, D. G. García, J. C. Ramirez and L. M. Lechuga, *Sensors*, 2016, **16**, 285.

2 L. Liu, M. Jin and Y. Shi, *Nanophotonics*, 2015, **4**, 419–436.

3 F. Vollmer and L. Yang, *Nanophotonics*, 2012, **1**, 267–291.

4 X. Fan, I. M. White, S. I. Shopova, H. Zhu, J. D. Suter and Y. Sun, *Anal. Chim. Acta*, 2008, **620**, 8–26.

5 A. B. González-Guerrero, J. Maldonado, S. Herranz and L. M. Lechuga, *Anal. Methods*, 2016, **8**(48), 8380–8394.

6 D. Martens and P. Bienstman, *Nanophotonics*, 2016, **4**, 4, DOI: 10.1515/nanoph-2016-0181.

7 T. Claes, W. Bogaerts and P. Bienstman, *Opt. Lett.*, 2011, **36**, 3320–3322.

8 M. Kitsara, K. Misiakos, I. Raptis and E. Makarona, *Opt. Express*, 2010, **18**, 8193–8206.

9 D. Martens, A. Subramanian, S. Pathak, M. Vanslembrouck, P. Bienstman, W. Bogaerts and R. Baets, *Photonics Technol. Lett.*, 2015, **27**(2), 137–140.

10 A. Z. Subramanian, P. Neutens, A. Dhakal, R. Jansen, T. Claes, X. Rottenberg, F. Peyskens, S. Selvaraja, P. Helin, B. Du Bois, K. Leyssens, S. Severi, P. Deshpande, R. Baets and P. Van Dorpe, *IEEE Photonics J.*, 2013, **5**(6), 2202809.

11 D. Martens, G. Dong and P. Bienstman, *Appl. Opt.*, 2017, **56**(5), 1286–1290.

12 P. K. Drain, L. Gounder, Fa. Sahid and M.-Y. S. Moosa, *Sci. Rep.*, 2016, **6**, 19992.

13 M. S. Murib, W. S. Yeap, Y. Eurlings, B. van Grinsven, H.-G. Boyen, B. Conings, L. Michiels, M. Ameloot, R. Carleer, J. Warmer, P. Kaul, K. Haenen, M. J. Schöning, W. De Ceuninck and P. Wagner, *Sens. Actuators, B*, 2017, **230**, 260–271.

14 E. T. Vandenberg, L. Bertilsson, B. Liedberg, K. Uvdal, R. Erlandsson, H. Elwing and I. Lundström, *J. Colloid Interface Sci.*, 1991, **147**, 103–118.

15 K. van der Maaden, K. Sliedregt, A. Kros, W. Jiskoot and J. Bouwstra, *Langmuir*, 2012, **28**, 3403–3411.

16 I. M. Klotz, in *Methods in Enzymology*, ed. C. H. W. Hirs, Academic Press, New York, 1967, vol. 11, p. 576.

17 S. K. Vashist, A. G. Venkatesh, E. M. Schneider, C. Beaudoin, P. B. Luppa and J. H. T. Luong, *Biotechnol. Adv.*, 2016, **34**(3), 272–290.

18 M. Soler, M. C. Estevez, M. Alvarez, M. A. Otte, B. Sepulveda and L. M. Lechuga, *Sensors*, 2014, **14**, 2239–2258.